Environmental Modelling of Ionic Mass Transfer Coefficient in a Unique Electrocoagulation Reactor

Safaa K. Hashim Al-Khalaf *(**), Ahmed Samir Naje*†, Zaid Abed Al-Ridah* and Haider M. Zwain*
*Collage of Engineering, AL-Qasim Green University, Babylon 51031, Iraq
**Faculty of Engineering, University of Kufa, Al-Najaf, Iraq
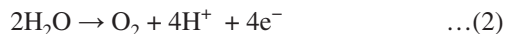†Corresponding author: Ahmed Samir Naje: ahmednamesamir@yahoo.com

ABSTRACT

Ionic mass transfer in a novel electrocoagulation reactor (ECR) using a rotating impeller anode is studied experimentally using the limiting current density method. The CFD simulation is also conducted for characterizing the novel electrocoagulation reactor (ECR) and validating the experimental study of ionic mass transfer. Variables included rotational speed and anode diameter. The Bland-Altman method was used to verify the accuracy of experimental and simulation results. Data for the condition $11852 < Re < 58550$ and $88 < Sc < 285$ were found to fit the equation for the largest diameter of 11.2 cm; $Sh = 2.1Re^{0.93}Sc^{0.33}$. Based on COD removal efficiency, optimal EC performance is realized at the largest anode diameter of 11.2 cm, confirming the enhancement of aluminum mass transfer by increasing the anode diameter. The experimental values of current density and mass transfer coefficient are validated by CFD simulation for all the rotational speeds and anode diameters. The accuracy is up to 95% for the experimental current densities compared with simulation values.

INTRODUCTION

Electrochemically assisted coagulation involves in situ generations of coagulants through an electrode solution of a sacrificial anode, which is usually composed of iron or aluminum. The reactions in an electrocoagulation cell are summarized in Eqs. (1) to (3), with the oxidation of the metallic anode (M = Fe or Al) and reduction of water as the main electrochemical reactions. In the reactions, oxidation occurs at the anode, and water reduction occurs through the electrocoagulation reactions (Chen 2004).

At the anode:

$$M \rightarrow M^{3+} +\ 3e^- \qquad \cdots(1)$$

$$2H_2O \rightarrow O_2 + 4H^+ +\ 4e^- \qquad \ldots(2)$$

At the cathode:

$$H_2O + e^- \rightarrow 1/2H_2 + OH^- \qquad \ldots(3)$$

Creating turbulence via an electrocoagulation (EC) reactor reduces the electrode inter-resistance drop (IR-drop) and improves the performance of the current using either a mixer with static or rotating electrodes. This trend may be alleviated by enhancing mass transfer towards increasing turbulence (Mollah et al. 2004). Mass transfer monitoring is essential for electrocoagulation reactors, which leads to mass transfer measurements (MTMs). The MTMs can be conducted by employing several electrochemical reactor geometries, with three-dimensional porous electrodes and a parallel plate or rotating electrodes. The reactors often operate during partial or complete mass transfer control. This trend is due to the controlled rate of convection diffusion of the reactant from the surface of the electrode to the bulk of the solution. The EC technology that involves the control of mass transfer has numerous applications in different fields of study. The fields include electrosynthesis, photocatalysis, metal recovery, effluent treatment, and energy conversion and storage (Eisenberg et al. 1954, Ponce-de-Leon et al. 2007). In the EC process, the limiting current is an essential determinant for the analysis of rates of mass transfer. When the limiting current controls the EC system, the comparison of that system with other electrochemical systems can help in determining the hydrodynamic characteristics for better removal efficiencies of pollutants. The following equations are employed to determine the mass transfer behavior in the EC cell or reactor involving mass transfer coefficients (K_m) for the anode oxidation, which are determined from the values of the limiting current Selman JR, Tobias CW. Mass-transfer measurements by the limiting-current technique (Adv et al. 1978, Burns & Jachuck 2005, Rong et al. 2007, Ibrahim et al. 2013, Abdel-Aziz et al. 2011, El-Shazly et al. 2013).

$$K_m = i_L/nFAC_b \qquad ,\ldots(4)$$

where i_t is the limiting current (A), F is Faraday's constant (96500 $C.mol^{-1}$), n is electron moles (3 for Al), A is the electrode surface area in cm^2, and C_b is the concentration of the bulk solution in $mol.cm^{-3}$.

Dimensionless numbers like the Reynolds number (Re), Schmidt number (Sc), and Sherwood number (Sh) are often used for different systems having rotating electrodes instead of superficial solution velocity and mass transfer coefficients. Below are the dimensionless numbers used:

$$Sh = K_m d/D, \qquad ...(5)$$

$$Re = \rho N d^2/\mu, \qquad …(6)$$

$$Sc = \mu/\rho D, \qquad …(7)$$

where D, d, N, μ, and ρ diffusion coefficient ($cm^2.s^{-1}$), represent effective diameter (cm), rotational speed (rps), fluid viscosity ($g.cm^{-1} \cdot s^{-1}$) and fluid density ($g.cm^{-3}$).

The experimental mass transfer data for a variety of ECR designs are correlated by using the dimensionless relationship (Rajeshwar & Ibanez 1997, Tamas et al. 2007):

$$Sh = bRe^a Sc^{0.33}, \qquad …(8)$$

where a is the Reynolds number exponent, which is dimensionless and b is the mass transfer correlation constant.

Several studies have used hydrodynamic voltammetry to determine the correlations of the mass transfer by using the potential ranges and the limiting current. Under such conditions, the reaction is mass transfer controlled in electrochemical systems using rotating disc electrodes (Tamas et al.2007, Ragnini et al. 2000, Lanza & Bertazzoli 2007) and rotating cylinder electrodes (Ponce-de-Leon et al. 2007, Grau & Bisang 2005, Grau & Bisang 2011). The main aims of this study are to investigate the mass transfer coefficients for a new model of EC reactor with rotating impeller anode at different rotational speeds and impeller diameters by experimental work and to validate by computational fluid dynamic (CFD) simulation to reveal the importance of mass transfer in electrocoagulation processes. The model and experiments focus on an EC process using a rotating electrode. The Bland-Altman statistical method has been used to verify the experimental results.

MATERIALS AND METHODS

Experimental Setup

Fig. 1 presents the experimental setup used for the novel electrocoagulation reactor. The volume of the stirred tank reactor was 10 liters, made from Perspex. The reactor came with a rotating shaft with a diameter of 32 mm, to sustain the impeller and sustain the rotational speed of the mounted electrode. The electrode is made of aluminum. The designed

rotational speed of the electrode varies from 75, 100, 150, 200, to 250 rpm. 10 impellers were used with a rotating anode and 10 rings as the cathode. In the design, the impeller consisted of 4 rods each with dimensions of 30 mm and 12 mm as the length and diameter, respectively. The dimensions of each ring were as 172 mm, 134 mm, and 12 mm, the outer diameter, internal diameter, and thickness, respectively. The rings were kept 30 mm apart and 500 cm^2 as the active surface area of the reactor. Three baffles (equally spaced) were used in the reactor. Further details on experimental procedure and design can be found in previous work (Naje 2019). Table 1 enlightens the main properties of wastewaer collected from a textile manufacturer in Babylon, Iraq.

Computational Fluid Dynamics Modelling

The three-dimensional Solid Oxide Fuel Cell (SOFC) model built in commercial CFD software ANSYS 15.0 was used. The numerical model was completed to resemble the experimental setup used. The model considers all the complex electro-thermo-chemical characteristics by simulation of the complex processes in the SOFC operations. The working principle of the SOFC model is compatible with electrochemical reactions (Puthran 2011). Further details on the model and procedure for the model development are as under.

The Model

The modeling strategy is detailed in the official manual of Ansys[R] (Eickhoff & Roeser 2009). The SOFC model numerically solves a set of partial differential equations (PDE) contained in SOFC theory. The PDE equations involve mass transfer via the flow channels, the fuel flow, the electrodes, and the chemical and electrochemical reactions that occur in the SOFC system (O'Hayre et al. 2006). The potential field in the conductive layers of the cell depends on the electrical model. The computational mesh generated for the model is shown in Fig. 2 (a and b).

Computational Model Theory

The following cell phenomenon is required for the understanding and development of the SOFC (Singhal & Kendall 2003):

Table 1: Characteristics of textile wastewater.

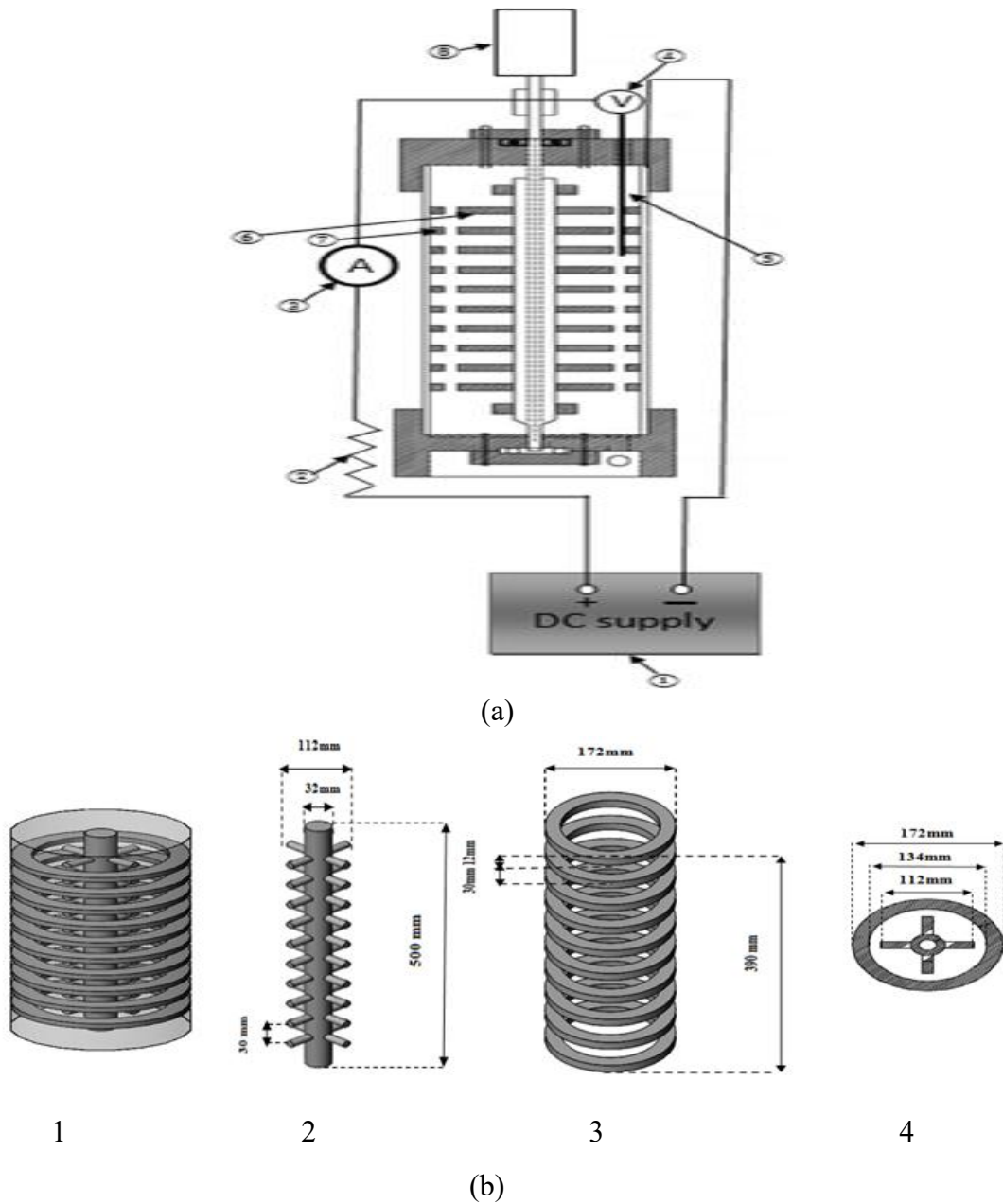| Parameters	Values
Electrical conductivity [$\mu S.cm^{-1}$]	1450
pH	4.52
Density [$g .cm^{-3}$]	0.997
Absolute viscosity [$g.cm^{-1}.s^{-1}$]	0.0089
COD [$mg.L^{-1}$]	990

(a)

1   2   3   4

(b)

Fig. 1: (a). Schematic view of EC experimental setup (1) DC power supply; (2) variable resistance; (3) multirange ammeter; (4) voltmeter; (5) reference electrode; (6) rotating impellers anode; (7) rings of cathode; (8) variable speed motor. (b). Configurations of electrodes (1) anode and cathode; (2) impellers of the anode; (3) rings of the cathode; (4) top view of impellers anode and rings cathode.

1. The ions and electrons transfer, as well as the computation of the cell potential and the current obtained under current and potential field transport.

2. The electrochemical reactions taking place at the electrodes.

3. The mass transfer involving mass conservation and species conservation.

4. The flow channels of the fluid (for both the non-porous and porous media.

The conservation equations are used to solve this phenomenon using the finite volume technique in combination with an implicit discretization scheme. The following assumptions were made to solve these equations (Srinivasan 2006):
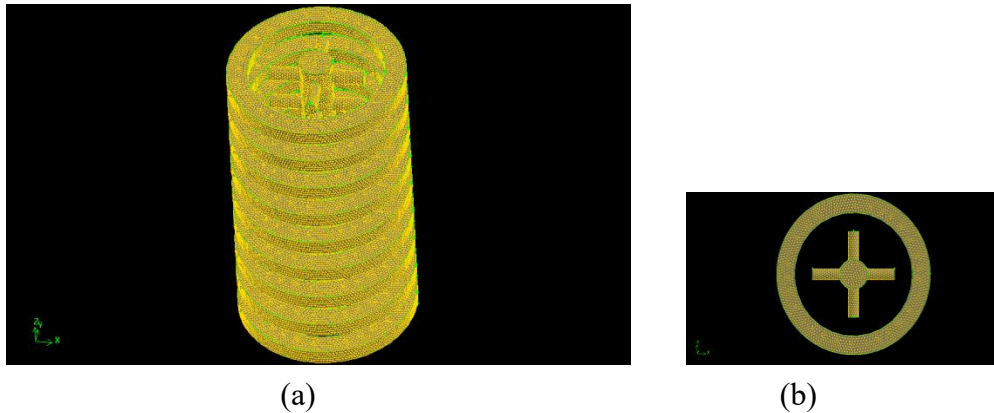
Fig. 2: Mesh structure representation of EC model with rotating anode (a) Whole geometry; (b) Top view of anode and cathode.

1. All the components exhibit similar thermal expansions, neglecting the effects of radiation heat transfer, and considering the single-cell model.
2. The reactions occur in a single step.
3. The principle of conservation of momentum for the model mass flow by zones in the cell operation is presented in Eq. 9.

$$\frac{\partial}{\partial t}\rho\vec{v} + \nabla.\rho\vec{v}y_i = \nabla.\vec{J}_i + S_{S,i} \qquad ...(9)$$

The effective binary diffusion coefficient is determined for the electrodes based on the tortuosity and porosity of the electrode matrix. The effective binary diffusion coefficient is given by Eq. 10.

$$D_{ij,eff} = \frac{\varepsilon}{\tau}D_{ij} \qquad ...(10)$$

The principle of conservation of charge used for conductive regions is expressed as

$$\nabla.i = 0 \qquad ...(11)$$

Where, i is:

$$i = -\sigma\nabla\phi \qquad ...(12)$$

The Laplace equation is employed as a governing principle to solve the species conservation equation.

$$\nabla \sigma\nabla\phi = 0 \qquad ...(13)$$

When the current is applied, there is a reduction in aluminum to Al^{+3} ions, flowing through the electrolyte. The release of electrons takes place through electrochemical reactions. These electrons flow through the current collector-connected external circuit. A potential difference is developed across two electrodes when electron transfer produces a current through the circuit. Nernst Equation was used to compute the output voltage of the cell (ANSYS Manual 15.0), and the

setting up of boundary conditions by electric potential value at the anode-impeller which means the reference potential of aluminum and the potential at the cathode-ring is varied. The single-cell structure temperature profile is demonstrated with the energy conservation equation in Eq.14.

$$\frac{\partial}{\partial t}\rho E + \nabla.\vec{v}\rho E + p = \nabla.(k_{eff}\nabla T - \sum_j h_j\vec{J}_j + \overline{\overline{\tau}}_{eff}.\vec{v}) + S_h$$
$$...(14)$$

Where S_h is the volumetric sink or source of energy and,

$$E = h - \frac{p}{\rho} + \frac{v^2}{2} \qquad ...(15)$$

And

$$h = \sum_j Y_j h_j \qquad ...(16)$$

The enthalpy flux terms are added to the energy equation accounting for the electrochemistry. The overall energy balance for the production of hydrogen and the corresponding enthalpy of formation is presented in Eq. 17 and 18, respectively.

$$\dot{Q}'' = h_{H_2}'' + h_{O_2}'' - h_{H_2O}'' - i\nabla V \qquad ...(17)$$

$$h_{H_2} = \dot{m}_{H_2}[\int_{T_{ref}}^{T} C_p dT + h_0] \qquad ...(18)$$

The effects of electrode potential voltage are taken into account in the energy equation. The Butler-Volmer equation can be used to obtain the interface current density. Therefore, the rate of reaction could be written in terms of the exchange current density as follows:

$$i = i_{0,eff}[e^{\frac{\alpha_a n\eta_{act,a}F}{RT}} - e^{\frac{-\alpha_c n\eta_{act,c}F}{RT}}] \qquad ...(19)$$

Where,

$$i_{0,eff} = i_{0,ref}(\frac{\chi_j}{\chi_{j.ref}})^{\gamma_j}$$

...(20)

The effective exchange current density is determined for the cathode side and the anode side. Considering the anode side:

$$i_{0,eff}^{anode} = i_{0,ref}^{anode}(\frac{\chi_{H_2}}{\chi_{H_2.ref}})^{\gamma_{H_2}}(\frac{\chi_{H_2O}}{\chi_{H_2O.ref}})^{\gamma_{H_2O}}$$

...(21)

Considering the cathode side,

$$i_{0,eff}^{cathode} = i_{0,ref}^{cathode}(\frac{\chi_{O_2}}{\chi_{O_2.ref}})^{\gamma_{O_2}}$$

...(22)

Newton's method can be used to solve the Butler-Volmer equation after the initial input of anode potential voltages. The values of current density are dependent on potential voltage. The production rate of the species helps to compute the concentration dependence of the species on the current-potential voltage characteristics of the cell are used to model the electrochemical reactions.

$$S = -\frac{ai}{nF}$$

...(23)

To measure the source terms for the equations, the underlying electrochemistry in equation 23 can be used with the conventions and the inputs to the governing equations' definition of basic initial parameters required. The initial current of the system determined from the applied potential voltage can be specified using the CFD module. The present simulation uses the initially specified potential voltage of the anode to find out the developed current of the system for each rotational speed and anode diameter.

Boundary Conditions Simulation Setup

The initial boundary conditions must be paired with the instance of the anode diameter. It is daunting to get the parameters required to set up a replica of the experimental setup. The available conditions and approximate values for the other parameters were used to develop the model. Anode rotational speeds are given as boundary conditions for the present model. The rotational speed is followed for the three impeller diameters of 9.2cm, 10.2cm, and 11.2cm. The operation was performed at atmospheric pressure, temperature room, and solution conductivity, density, and viscosity as mentioned in Table 1.

RESULTS AND DISCUSSION

Experimental Outcomes

The experimental results used in this study are from previous studies (Naje 2019). Results brought to light that the highest mass transfer coefficient was observed at the highest impeller anode diameter of 11.2 cm used. The Sherwood number estimated for different impeller diameters and the rotational speeds by plotting ($Sh/Sc^{0.33}$) versus Reynolds number (Eq. 6), is exhibited in Fig. 3. The following correlations were obtained by fitting data at different impeller anode diameters:

If d = 0.092 m,

$$Sh = 2.09\ Re^{0.89}Sc^{0.33}.$$ (25)

If d = 0.102 cm,

$$Sh = 2.1Re^{0.91}Sc^{0.33}.$$ ...(26)

If d = 0.112 cm,

$$Sh = 2.1Re^{0.93}Sc^{0.33}.$$ ...(27)

If $11852 < Re < 58550$ and $88 < Sc < 285$, 0.98 is the correlation coefficient.

It can be observed from the determined correlations that exponents of Re increase with an increase in anode diameter. The exponent values together with heading constant (b = 2.1) were greater than the previously reported values for rotating cylinder electrode ($Sh = 0.079\ Sc^{0.356}\ Re^{0.7}$) and rotating disk electrode ($Sh = 0.01\ Sc^{0.33}\ Re^{0.87}$), for turbulent flow. The value of the factors (a and b) are influenced by the geometric design of the electrode, indicating a higher mass transfer coefficient in comparison with the rotating disk or cylinder (Abdel-Aziz et al. 2011, Yanez-Varela et al. 2020).

CFD Simulation Outcomes

The flow physics and the various electrochemical reactions have been simulated from the CFD software. The various contours are plotted to analyze the changes happening in the electrochemical behavior inside the EC reactor with a rotating anode. The various rotational speeds for the three impeller anode diameters give information about their influence on the current density/intensity.

The contour of current density in Fig. 4 for 0.5V potential voltage, 150 rpm rotational speed, and 9.2cm anode diameter shows the maximum change happening in the place of the impeller's anode. There is nominal change throughout excluding the impeller as is noticed in the EC reactor. In the case of potential voltage, as shown in Fig. 5. Maximum voltage was observed at the wall of the cathode rings, whereas minimum voltage in the impeller, and a medium voltage throughout as expected by the behavior of the electrochemical system (Ra-
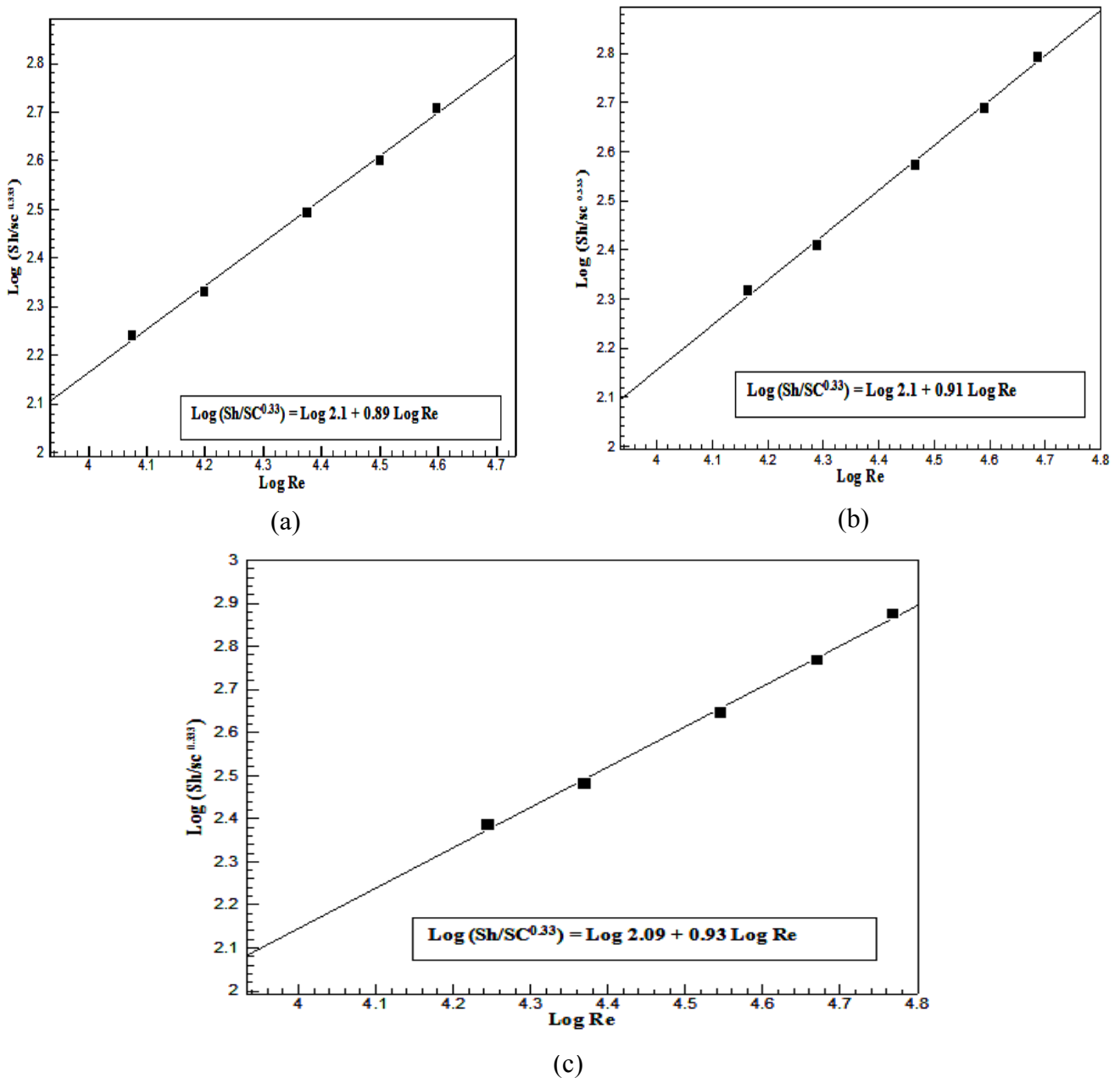
$$Log (Sh/SC^{0.33}) = Log\ 2.1 + 0.89\ Log\ Re$$

(a)

$$Log (Sh/SC^{0.33}) = Log\ 2.1 + 0.91\ Log\ Re$$

(b)

$$Log (Sh/SC^{0.33}) = Log\ 2.09 + 0.93\ Log\ Re$$

(c)

Fig. 3: Sherwood-Reynolds correlation for rotating impeller anode (a) d=9.20cm; (b) d=10.20cm; (c) d=11.20 cm.

jeshwar & Ibanez 1997, Rodriguez et al. 2003, Yanez-Varela et al. 2020).

The relationship of current density versus potential voltage for an impeller diameter of 9.2cm follows an increasing trend, as shown in Fig. 6. The current intensity increases when the potential difference increases for the rotational speed of 75rpm, till a potential difference of 2500 mV is reached. After that, it remains constant for any changes in potential difference. The nature of the curves for 100, 150, 200, and 250 rpm are the same starting 75rpm however begin at an expanding slope than the latter. The expanding of slope because of increment of limiting current with the increasing of anode rotational speed. For each rotational speed and anode diameter, CFD simulation values are

consistent with the experimental values. Fig. 7 explains the limiting current densities for each impeller anode diameter and rotational speed. The results show limiting current densities increased with increasing rotational speed and also the impeller's anode diameter. The results are presented in Fig. 5, 6, and 7, under the same potential voltage and increment of anode diameter or rotational speed. The current flow increases, resulting in the acceleration of the

EC reaction response. This behavior is perfect with the consequences of experimental results and former studies (González-Neria et al. 2021, Mora et al. 2016). The coefficient of mass transfer of ionic Al was enhanced by increasing the rotation speed and diameter of an anode, as shown in Fig. 8. The mass transfer coefficients obtained by CFD simulation are compatible with the experimental values.
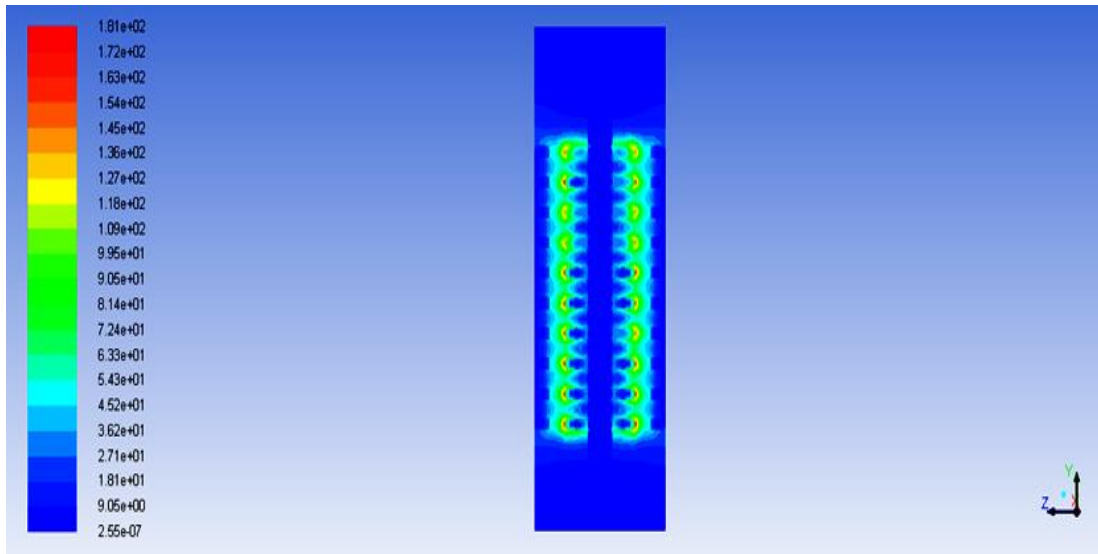

Fig. 4: Contours of current density (A.m^{-2}) in case of potential voltage is 0.5V in case of rotating speed =150 rpm and anode diameter = 9.2cm at x=0 section.
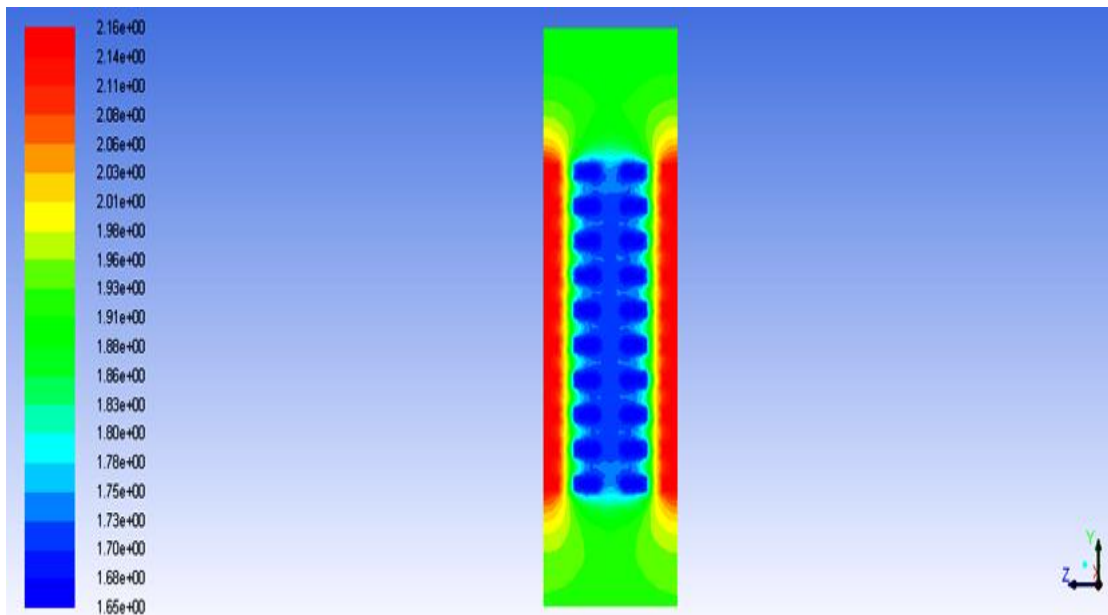

Fig. 5: Contours of potential voltage in case of rotating speed =150 rpm and anode diameter = 9.2cm at x=0 section.

Outcomes Verification

A statistical method is employed to confirm the measured limiting current of experimental work with CFD simulation values for each impeller's anode diameter and rotational speed. The Bland–Altman method is one of the statistical methods utilized for this purpose (Mendez et al. 2018, Tesche et al. 2018).

The data were collected from the developed devices based on the comparison with data obtained from the simulation or validated devices. This technique is based on the mean difference between the simulation and the developed instrument or system. The value of the mean difference will limit the acceptable area of the data that is generated by subtraction or addition of the standard deviation (SD) (González-Landaeta et al. 2008). This method will evaluate the parameters that affect the performance of the model design (device) in the zone of standard deviation limit as the acceptable area of the distribution of the measured data (Martínez-Delgadillo et al. 2013). Any design device is pronounced as good in
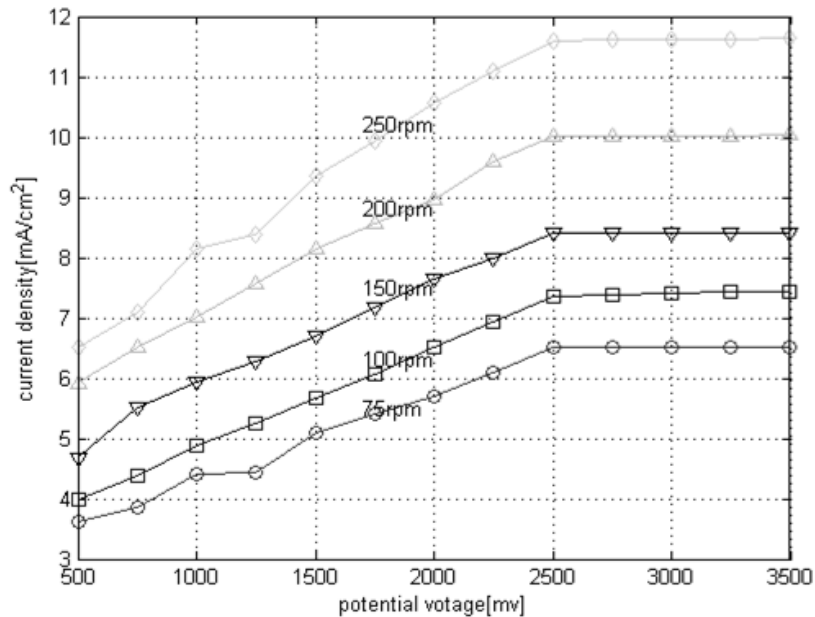

Fig. 6: Simulation current-potential voltage curves at an anode diameter of 9.20cm.
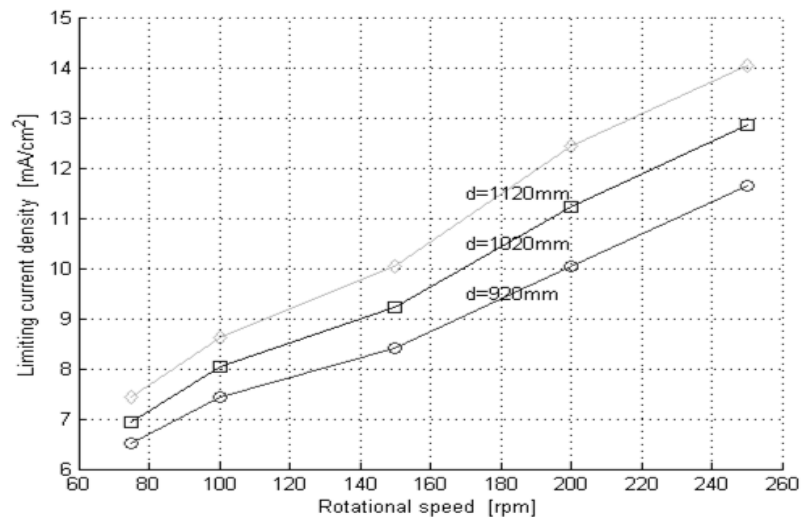

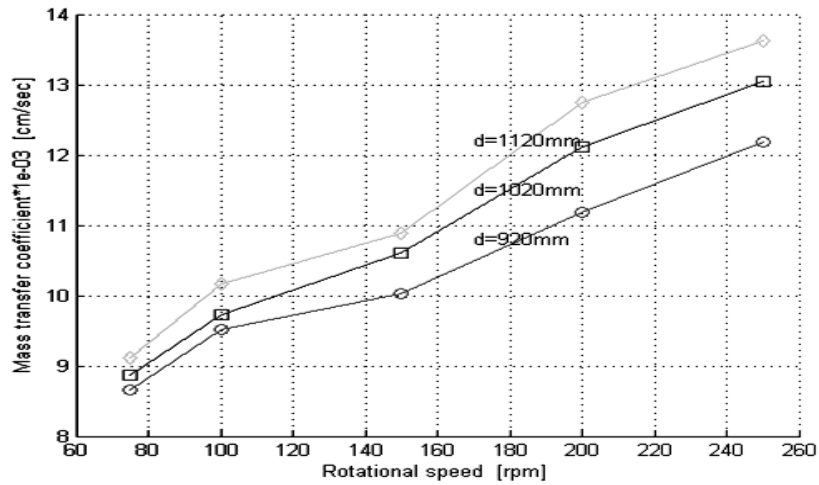Fig. 7: Simulation limiting current density for different anode diameters.

Fig. 8: Simulation mass transfer coefficient for different anode diameters.

performance if any measured data should be more than 95% potentially measured the data and the error must be less than 5% whereby the error boundary limits are via mean ± 2×SD stated by (Su et al. 2014).

Three impellers anode diameters (9.2, 10.2, and 11.2cm) are considered in measuring current (A), and the rotational speeds are 75, 100, 150, 200, and 250rpm. Fig. 9 (a), (b), and (c) indicated the distribution measured zone via standard deviation error for each anode diameter at optimal rotational speed (150 rpm). From Figs. 5, 6, and 7, it is seen that most of the measured current values in the mean of the 2×SD as required and the accuracy of these values between the
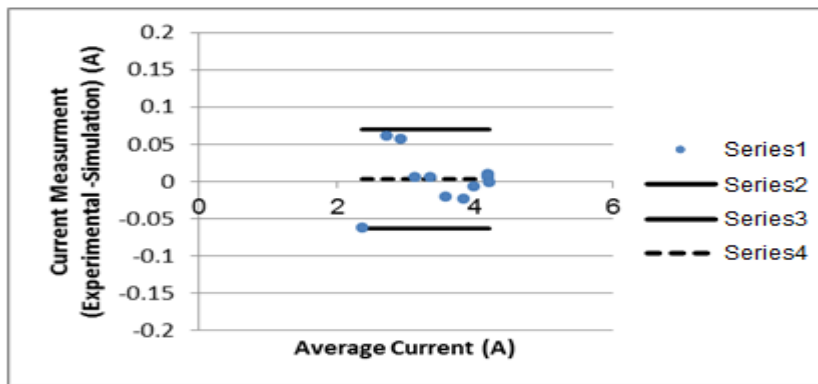
(a)
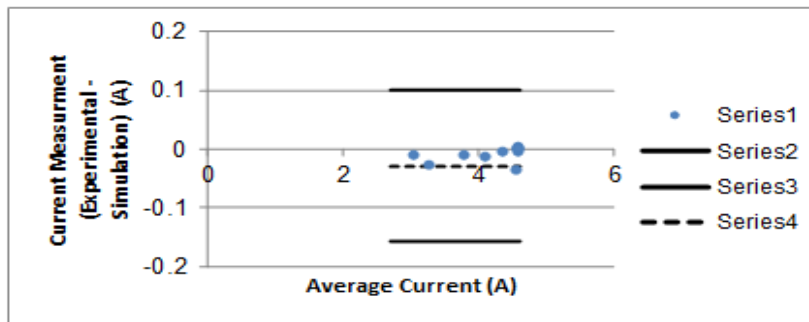
(b)
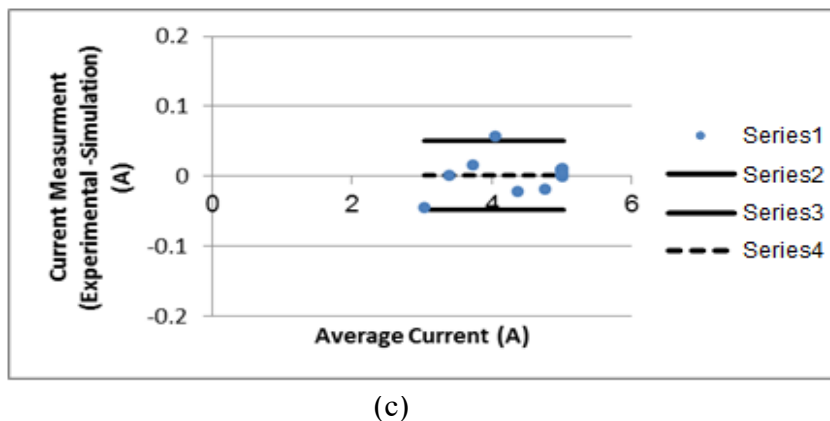
(c)

Fig. 9: Measured current verification between experimental and simulation work at 150 rpm with impellers anode diameter: (a). 9.2cm; (b). 10.2cm; (c). 11.2cm.

experiment and the CFD simulation has achieved a good agreement up to 95% for each anode diameter at 150 rpm.

CONCLUSIONS

The results show that increasing the impeller anode diameter and rotation speed increases the limiting current density. The results of the correlations using Reynolds and Sherwood numbers show that the optimum coefficient of mass transfer for experimental and simulated data is found at 11.2 cm of the impeller anode diameter. Where the correlation is as $Sh = 2.1Re^{0.936} Sc^{0.33}$). The current densities from CFD simulation show values close to that of the experimental data for all the anode diameters and rotation speeds employed. According to the Bland–Altman method, the accuracy is up to 95% for the experimental current density values.

ACKNOWLEDGMENT

REFERENCES

Abdel-Aziz, M., El-Shazly, A., Farag, H. and Sedahmed, G. 2011. Mass transfer behavior of rotating square cylinder electrochemical reactor in relation to wastewater treatment. Energy Conv. Manag., 52: 2870-2875.

Burns, J. and Jachuck, R. 2005. Determination of liquid-solid mass transfer coefficients for a spinning disc reactor using a limiting current technique. Int. J. Heat Mass Transf., 48: 2540-2547.

Chen, G. 2004. Electrochemical technologies in wastewater treatment. Sep. Purif. Technol., 8:11-41.

Eickhoff, J. and Roeser, H.P. 2009. Simulating Spacecraft Systems. Springer, Cham.

Eisenberg, M., Tobias, C. and Wilke, C. 1954. Ionic mass transfer and concentration polarization at rotating electrodes. J. Electrochem. Soc., 101: 306-320.

El-Shazly, A., Al-Zahrani, A. and Alhamed, Y. 2013. Kinetics and performance analysis of batch electrocoagulation unit used for the removal of a mixture of phosphate and nitrate ions from industrial effluents. Int. J. Electrochem. Sci., 8: 3176-3185.

González-Neria, I., Yáñez-Varela, J.A., Martínez-Delgadillo, S.A., Rivadeneyra-Romero, G. and Alonzo-Garcia, A. 2021. Analysis of the turbulent flow patterns generated in isotropic porous media composed of aligned or centered cylinders. Int. J. Mech. Sci., 199: 106396.

Grau, J. and Bisang J. 2011. Mass-transfer studies at rotating cylinder electrodes with turbulence promoters. Chem. Eng. Process Intensif., 50: 940-943.

Grau, J. and Bisang, J. 2005. Mass transfer studies at rotating cylinder electrodes of expanded metal. J. Appl. Electrochem., 35: 285-291.

Ibrahim, D.S., Veerabahu, C., Palani, R., Devi, S. and Balasubramanian, N. 2013. Flow dynamics and mass transfer studies in a tubular electrochemical reactor with a mesh electrode. Comp. Fluids, 73: 97-103.

Lanza, M. and Bertazzoli, R. 2000. Removal of Zn (II) from chloride medium using a porous electrode: current penetration within the cathode. J. Appl. Electrochem., 30: 61-70.

Martínez-Delgadillo, S.A., Gutiérrez-Torres, C. and Jiménez-Bernal J. 2013. Determination of the spatial distribution of the turbulent intensity and velocity field in an electrochemical reactor by CFD. Int. J. Electrochem. Sci., 8: 274-289.

Mendez, V., Di Giuseppe, M. and Pasta, S. 2018. Comparison of hemodynamic and structural indices of ascending thoracic aortic aneurysm as predicted by 2-way FSI, CFD rigid wall simulation, and patient-specific displacement-based FEA. Comp. Biol. Med., 100: 221-229.

Mollah, M.Y., Morkovsky, P., Gomes, J.A., Kesmez, M., Parga, J. and Cocke, D.L. 2004. Fundamentals, present and future perspectives of electrocoagulation. J. Hazard. Mater., 114: 199-210.

Mora, M.M., Vergara, C.P., Leiva, M.A., Delgadillo, S.M. and Rosa-Dominguez, E.R. Life cycle assessment of carbon capture and utilization from ammonia process in Mexico. J. Environ. Manag., 183: 998-1008.

Naje, A.S. 2019. Enhancement of ionic mass transfer coefficient using a unique electrocoagulation reactor with a rotating impeller anode. Sep. Sci. Technol., 9: 1-10.

O'Hayre, R.P., Cha, S.W., Colella, W. and Prinz, F.B. 2006. Fuel Cell Fundamentals: John Wiley & Sons, New York.

Ponce-de-Leon, C., Low, C., Kear, G. and Walsh, F. 2007. Strategies for the determination of the convective-diffusion limiting current from steady-state linear sweep voltammetry. J. Appl. Electrochem., 37: 1261-1270.

Puthran, S.L. 2011. 3-Dimensional Computational Fluid Dynamics Modeling of Solid Oxide Fuel Cell Using Different Fuels. DTIC Document.

Ragnini, C.A., Di Iglia, R.A., Bizzo, W. and Bertazzoli, R. 2000. Recycled niobium felt as an efficient three-dimensional electrode for electrolytic metal ion removal. Water Res., 34: 3269-3276.

Rajeshwar, K. and Ibanez, J.G. 1997. Environmental Electrochemistry: Fundamentals And Applications in Pollution Sensors and Abatement: Academic Press, Cambridge, MA

Rodriguez, M.G., Aguilar, R., Soto, G. and Martínez, S.A. 2003. Modeling an electrochemical process to remove Cr (VI) from rinse water in a stirred reactor. J. Chem. Technol. Biotechnol., 78: 371-36.

Rong, X., Haiyan, F., Peng, Z. and Heping, G. 2007. Measurement of enhanced mass transfer coefficient in the tube by limiting diffusion current technique. Petrochem. Technol., 36: 712.

Selman, J.R. and Tobias, C.W. 1978. Mass-transfer measurements by the limiting-current technique. Adv. Chem. Eng., 10: 311-318.

Singhal, S.C. and Kendall, K. 2003. High-Temperature Solid Oxide Fuel Cells: Fundamentals, Design, and Applications. Elsevier, Netherlands.

Srinivasan, S. 2006. Fuel Cells: From Fundamentals to Applications. Springer Science & Business Media, Netherlands.

Su, Y., Zhang, Y., Jin, Y., Yao, Y., Zhang, R. and Jiang, Y. 2014. The feasibility of the dicrotic augmentation index to replace the tidal augmentation index. Information and Automation (ICIA), 2014 IEEE International Conference, pp. 943-948.

Tamas, A., Martagiu, R. and Minea, R. 2007. Experimental determination of mass transfer coefficients in dissolution processes. Chem. Bull. Polit. Univ. Timisoara, 52: 133-138.

Tesche, C., De Cecco, C.N., Baumann, S., Renker, M., McLaurin, T.W., Duguay, T.M. and Schoepf, U.J. 2018. Coronary CT angiography–derived fractional flow reserve: machine learning algorithm versus computational fluid dynamics modeling. Radiology, 288(1): 64-72.

Yanez-Varela, J.A., Alonzo-Garcia, A., Gonzalez-Neria, I., Mendoza-Escamilla, V., Rivadeneyra-Romero, G. and Martinez-Delgadillo, S.A. 2020. Experimental and numerical evaluation of the performance of the electrochemical reactor operated with static and dynamic electrodes in the reduction of hexavalent chromium. Chem. Eng. J., 390: 124575.